Research Article

Multiple slip effects on MHD unsteady viscoelastic nano-fluid flow over a permeable stretching sheet with radiation using the finite element method

Shahid Ali Khan[1] · Yufeng Nie[1] · Bagh Ali[1]

Received: 17 August 2019 / Accepted: 30 November 2019 / Published online: 11 December 2019

Abstract
The current study investigates the impact of multiple slips on Jeffrey fluid model for unsteady magnetohydrodynamic viscoelastic buoyant nanofluid in the presence of Soret and radiation over a permeable stretching sheet. Appropriate transformations are utilized to obtain the relevant nonlinear differential system. The obtained differential system is tackled numerically with the finite element method. Effect of the controlling parameters on dimensionless quantities such as velocity, temperature, concentration, and nano-fluid volume fraction profile, as well as on dimensionless numbers such as local Nusselt, Sherwood, nano-particle Sherwood, and the local friction coefficient is analyzed. The effect of multiple slips is examined and found that the boundary layer flow increases in the presence of multiple slips. Numerically obtained solutions are contrasted with the published literature and found to be in nice agreement. The present study has many applications in coating and suspensions, cooling of metallic plate, paper production, heat exchangers technology, and materials processing exploiting.

Keywords MHD · Multiple slip · Viscoelastic buoyant nanofluid · Radiation · Finite element method

1 Introduction

In recent technological advances, the study of non-Newtonian materials has caught the attention of engineers and scientists. Broad stimulation of scientists is due to the wide use of liquids in technology and in industry. Examples of such applications are paints, colloids and suspensions, cosmetics, polymer solutions, foods, exotic lubricants, paper production, coal water, ketchup, glues, ink, blood, some oils, fiber technology and clay coating. Due to the diversity of non-Newtonian liquids, there is no law to explain the viscous and elastic properties of these liquids. Despite all these challenges, researchers have made valuable contributions to current literature on a variety of non-Newtonian fluids [1–8]. Among them, visco-elastic fluids are expected to be more important in the current research area due to their extensive applications in engineering and industrial production. Some of the most recent practices in this regard are in Kumar et al. The effect of non-linear thermal radiation on the flow of the mixed visco-elastic nano-liquid double diffusion convection boundary layer is discussed on a stretch film. Convective heat transfer and the MHD visco-elastic nanofluid flow induced by a stretch film are studied by Shit et al. [9]. Sheikholeslami et al. [10] studied the impact of the magnetic field and thermal radiation on the hydrothermal behavior of nanofluids of Fe_3O_4–H_2O. The impact of Lorentz forces on the flow of CuO–water nanofluids in a permeable housing is presented by CVFEM and Nanofluid fluxes and heat transfer in a cavity. magnetic field from Sheikholeslami et al. [11, 12]. The flow of the magnetohydrodynamic boundary layer (MHD) with a stagnation point on a visco-elastic liquid stretch film in

✉ Yufeng Nie, yfnie@nwpu.edu.cn | [1]Department of Applied Mathematics, School of Science, Northwestern Polytechnical University, Dongxiang Road, Chang'an District, Xi'an 710129, China.

the presence of thermal radiation was studied by Naryana et al. Application of the law of Darcy to the flow of nanofluids in a porous cavity below impact of Lorentz forces investigated by Sheikholeslami et al. Hussanan et al. [13] investigated the analytical solution for the suction and injection flow of a visco-elastic Cassco fluid past a stretch surface in the presence of viscous dissipation. Majeed et al. [14] investigated the analysis of heat transfer in a ferromagnetic visco-elastic fluid stream on a stretching sheet.

Non-Newtonian liquids have been discovered a lot of significant and helpful for innovative perspectives, for example, multi-grade oils, fluid cleansers, paints, polymer arrangements, and polymer softens are talked about in Elahi [15]. Moreover, ongoing advances in nanotechnology have prompted the improvement of another imaginative class of warmth move called nanofluids made by scattering nanoparticles. Non-Newtonian nanofluids are generally experienced in numerous modern and innovation applications, for instance melts of polymers, natural arrangements, paints, tars, black-tops, and pastes, and so on. The form of nanofluids is essentially the dispersion of solid nanoparticles in liquids such as water, oil or ethylene glycol. These nanoparticles are usually made from metals, oxides and carbon nanotubes. Nanoparticles can also be used in biomedical applications such as magnetic resonance imaging, photothermal therapy, drug delivery control, protein separation, biosensor, DNA detection and immune sensors. Choi [16] presented for the first time an innovative mixing technique using nanoparticles and basic liquids, with the aim of improving heat transfer by increasing the thermal conductivity of the liquid.

Boungiorno [17] then explained the reasons for improving the heat transfer of nanofluids and concluded that Brownian diffusion and heat development were the reasons for this improvement. Some recent articles about nanomaterials are presented in the Refs. [18–23]. Sulochana et al. [24] investigated the magnetohydrodynamic radiation fluid thin film flux of a kerosene nanofluid with the aligned magnetic field. Daniel et al. [25] investigated the effects of slip and convection conditions on the flow of MHD nanofluids on a porous non-linear stretch / shrink film. The nanofluid streams in a microchannel with oblique cross-flow injection are being studied by Shriniy et al. [26].

The effect of exponentially varying viscosity and permeability on the Blasius current of the nanotile fluid on an electromagnetic plate through a porous medium is presented by Hakkem et al. [27] Waqas et al. [28] discussed the interaction of thermal radiation in hydromagnetic visco-elastic nanomaterials subject to gyrotactic microorganisms. Maleki et al. [29] investigated heat transfer and nano-liquid flow on a porous plate with radiation and slip limit conditions. The effects of the second-order nano-fluid poiseuille call plan under the influence of Stefan blowing into a channel are discovered by Alamri et al. [30]. The effects of thermal radiation and slip on the flow of the MHD stagnation point of non-Newtonian nano fluid on a convection stretch surface are being studied by Besthapu et al. [31].

Motivated by the aforementioned studies, the present paper aims to investigate investigates the effect of multiple slips on unsteady two-dimensional magnetohydrodynamic boundary layer flow of viscoelastic buoyant nanofluid with thermal radiation and Soret effect over a stretching sheet. Governed by an appropriate similarity transformation procedure partial differential equations are transformed into ordinary differential equations. The resulting ODE's is numerically solved by hybrid approach consisting of finite element method [32–40]. The consequences obtained were comprehensively discussed in tabulation and graphical representation.

2 Mathematical formulation

Consider the unsteady two-dimensional MHD boundary layer of an electrically conductive liquid immersed in visco-elastic floating nanofluid with multiple slips and thermal radiation on a linear stretching sheet. The flow of conductive fluid is caused by stretching the sheet in the direction $U(x,t) = ax/(1-\lambda t)$, where a is the stretch ratio and λ is the positive constant. Consider that there is no flux of nanoparticles on the wall and that the surface extends in the direction of y. Suppose T_w, ψ_w and C_w define the temperature, dissolved concentration and friction of the nanoparticles on the stretch sheet as follows:

$$T_w = T_\infty + T_0\left(\frac{ax}{2\nu(1-\lambda t)^2}\right)$$
$$C_w = C_\infty + C_0\left(\frac{ax}{2\nu(1-\lambda t)^2}\right)$$
$$\phi_w = \phi_\infty + \phi_0\left(\frac{ax}{2\nu(1-\lambda t)^2}\right)$$

where T_0, C_0 and ϕ_0 are the reference temperature, the reference solute concentration and the reference concentration of the nanoparticles, and T_∞ is the ambient temperature, C_∞ the concentration solutal and ϕ_∞ is supposed to be the concentration of nanoparticles. In the current study, $B(x) = B_0 x^{-1/2}$ summarizes the magnetic field input, where B_0 is a uniform magnetic field strength. According to the above hypothesis, the conservation of mass, linear momentum conservation, energy conservation, salt concentration and volume fraction of nanoparticles can be obtained as follows:

$$\frac{\partial u}{\partial x}+\frac{\partial u}{\partial y}=0, \tag{1}$$

$$\begin{aligned}&\frac{\partial u}{\partial t}+u\frac{\partial u}{\partial x}+v\frac{\partial u}{\partial y}\\&=\frac{\nu}{1+\lambda^*}\left[\frac{\partial^2 u}{\partial y^2}+\lambda_t\left(u\frac{\partial^3 u}{\partial x\partial y^2}+\frac{\partial u}{\partial x}\frac{\partial^2 u}{\partial y^2}\right.\right.\\&\left.\left.-\frac{\partial u}{\partial y}\frac{\partial^2 u}{\partial x\partial y}+v\frac{\partial^3 u}{\partial y^3}\right)\right]\\&-\frac{\sigma B^2(x)u}{\rho}+g\beta_T(T-T_\infty)+g\beta_C(C-C_\infty)\\&+g\beta_\phi(\phi-\phi_\infty)\end{aligned} \tag{2}$$

$$\begin{aligned}&\frac{\partial T}{\partial t}+u\frac{\partial T}{\partial x}+v\frac{\partial T}{\partial y}=\alpha\left(1+\frac{16T_\infty^3\sigma^*}{3k^*\kappa}\right)\frac{\partial^2 T}{\partial y^2}\\&+\tau\left[D_B\frac{\partial \psi}{\partial y}\frac{\partial T}{\partial y}+\frac{D_T}{T_\infty}\left(\frac{\partial T}{\partial y}\right)^2\right]-\frac{\sigma B^2(x)u}{\rho}\end{aligned} \tag{3}$$

$$\frac{\partial C}{\partial t}+u\frac{\partial C}{\partial x}+v\frac{\partial C}{\partial y}=D_s\frac{\partial^2 C}{\partial y^2}+D_{CT}\frac{\partial^2 T}{\partial y^2} \tag{4}$$

$$\frac{\partial \phi}{\partial t}+u\frac{\partial \phi}{\partial x}+v\frac{\partial \phi}{\partial y}=D_B\frac{\partial^2 \phi}{\partial y^2}+\frac{D_T}{T_\infty}\frac{\partial^2 T}{\partial y^2} \tag{5}$$

with respect to the boundary conditions

$$\begin{aligned}&u=U(x,t)+U_{slip}, v=v_w, T=T_w(x,t)+T_{slip},\\&C=C_w(x,t)+C_{slip},\\&\phi=\phi_w(x,t)+\phi_{slip}\quad at\ y\to 0\end{aligned} \tag{6}$$

$$u\to 0, T\to T_\infty, C\to C_\infty, \phi\to\phi_\infty,\quad as\quad y\to\infty, \tag{7}$$

where u and v are the speed components, x and y, ν, σ, ρ, respectively, the kinetic viscosity, electrical conductivity, and fluid viscosity. D_B, D_T, D_s are respectively Brownian diffusion, thermophoretic diffusion and sol solution. To solve the Eqs. (1)–(7) we have introduced the following transformations for agreements:

$$\begin{aligned}&\eta=\sqrt{\frac{a}{\nu(1-\lambda t)}}y,\quad \psi=\sqrt{\frac{a\nu}{(1-\lambda t)}}xf(\eta),\\&\theta(\eta)=\frac{T-T_\infty}{T_w-T_\infty}, S(\eta)=\frac{C-C_\infty}{C_w-C_\infty},\quad \gamma(\eta)=\frac{\phi-\phi_\infty}{\phi_w-\phi_\infty}\end{aligned} \tag{8}$$

Given the transformation equation, the partial non-linear differential equations (1)–(6) transform into the following non-linear ODE's system:

$$\begin{aligned}&f'''+\beta(2f'f'''-f''^2-ff^{iv})\\&+(1+\lambda)(ff''-f'^2-A\left[\frac{\eta}{2}f''+f'\right]\\&-Mf'+\lambda_1\theta+\lambda_2 S+\lambda_3\gamma)=0,\end{aligned} \tag{9}$$

$$\begin{aligned}&(1+R)\frac{1}{Pr}\theta''-f'\theta+f\theta'-A\left(\frac{\eta}{2}\theta'+2\theta\right)\\&+Nb\gamma'\theta'+Nt\theta'^2-Mf'=0\end{aligned} \tag{10}$$

$$\frac{1}{Sc}S''-f'S+fS'-A\left(\frac{\eta}{2}S'+2S\right)+S_r\theta''=0 \tag{11}$$

$$\gamma''-Le\left[f'\gamma-f\gamma'+A\left(\frac{\eta}{2}\gamma'+2\gamma\right)\right]+\frac{Nt}{Nb}\theta''=0 \tag{12}$$

and the transformed boundary conditions Eqs. (6) and (7) are:

$$\begin{aligned}&f(0)=f_w, f'(0)=1+S_f f''(0), \theta(0)=1+S_t\theta'(0),\\&S(0)=1+S_p S'(0),\\&\gamma(0)=1+S_g\gamma'(0),\end{aligned} \tag{13}$$

$$f'(\infty)\to 0, \theta(\infty)\to 0, S(\infty)\to 0, \gamma(\infty)\to 0, \tag{14}$$

The primes show the differentiation with respect to η. The parameters in Eqs. (9)–(12) $M=\frac{\sigma B_0^2}{\rho c_o}, Pr=\frac{\nu}{\alpha}, Nb=\frac{\tau D_B(\psi_w-\psi_\infty)}{\nu}$, $Nt=\frac{\tau D_T(T_w-T_\infty)}{\nu T_\infty}, Sc=\frac{\nu}{D_B}, Le=\frac{\sigma}{D_B}, R=\frac{16\sigma^* T^3_\infty}{3k_f k^*}, Sr=D_T T_0/\nu C_0$ are magnetic, Prandtl, Brownian, thermophoresis, Schmidt, Lewis number, thermal radiation and Soret number, respectively. $A=\lambda_t/a$ is the unsteady parameter and λ_t is the retardation time, $\lambda_1=g\beta_T T_0/a\nu$, $\lambda_2=g\beta_C C_0/a\nu$, $\lambda_3=g\beta_\phi\phi_0/a\nu$ are the buoyancy parameters and $\beta=\lambda_t a/(1-\lambda t)$ is the Deborah number, S_f is the hydrodynamic slip, S_t the thermal slip, S_p the solutal slip and S_g is considered to be the nano-particle slip condition. Expression for physical quantities of interest are local skin friction coefficient C_f, Nusselt number Nu, the Sherwood number Sh_x and the nano-particle Sherwood number $Sh_{x,n}$ are,

$$\begin{aligned}&C_f=\frac{\tau_w}{\frac{1}{2}\rho U_w^2}, Nu=\frac{xq_w}{\kappa(T_w-T_\infty)},\\&Sh_x=\frac{xq_m}{D_s(C_w-C_\infty)}, Sh_{x,n}=\frac{xq_{np}}{D_B(\phi_w-\phi_\infty)},\end{aligned} \tag{15}$$

$$\tau_w = \mu\left(\frac{\partial u}{\partial y}\right)_{y=0} + \lambda_t\left(u\frac{\partial^2 u}{\partial x \partial y} + 2\frac{\partial u}{\partial x}\frac{\partial u}{\partial y} + v\frac{\partial^2 u}{\partial y^2}\right),$$
$$q_w = -\alpha\left(\frac{\partial T}{\partial y}\right)_{y=0}, \tag{16}$$
$$q_m = -D_s\left(\frac{\partial C}{\partial y}\right)_{y=0}, q_{np} = -D_B\left(\frac{\partial \phi}{\partial y}\right)_{y=0}.$$

Plugging the values from (8) into (15)-(16), we can get

$$C_f(Re_x)^{\frac{1}{2}} = 2(1+3\beta f''(0)), \quad Re_x^{-1/2}Nu = -(1+R)\theta'(0),$$
$$Re_x^{-1/2}Sh_x = -S'(0), \quad Re_x^{-1/2}Sh_{x,n} = -\gamma'(0) \tag{17}$$

Where $Re_x = U_w x/\nu$ is the Reynolds number. The ordinary differential equations(ODE) are highly nonlinear, which are solved numerically by Hybrid finite element technique.

3 Finite element method solutions

The current problem is solved by using the finite element method(FEM). Due to the numerical integration, the error is minimized by using the hybrid technique inherent in FEM. As a result, this approach is expected to yield better and more effective results. The steps used in FEM are:

- Discretization of domain into small elements.
- Selection of appropriate shape function.
- Development of finite element equations.
- Assemble the element equations to obtain global equations.
- Incorporation of the boundary conditions.
- Solve the simultaneous equations for the unknowns .
- Interpolation of results (Fig. 1).

we assume

$$f' = h. \tag{18}$$

plugging Eq. (18) into Eqs. (9)–(14), we get

$$h'' + \beta(2hh'' - h'^2 - fh''') + (1+\lambda)(fh' - h^2 - A\left[\frac{\eta}{2}h' + h\right] - Mh + \lambda_1\theta + \lambda_2 S + \lambda_3\gamma) = 0, \tag{19}$$

$$(1+R)\frac{1}{Pr}\theta'' - h\theta + f\theta' - A\left(\frac{\eta}{2}\theta' + 2\theta\right) + Nb\gamma'\theta' + Nt\theta'^2 - Mh = 0, \tag{20}$$

$$\frac{1}{Sc}S'' - f'S + fS' - A\left(\frac{\eta}{2}S' + 2S\right) + S_r\theta'' = 0, \tag{21}$$

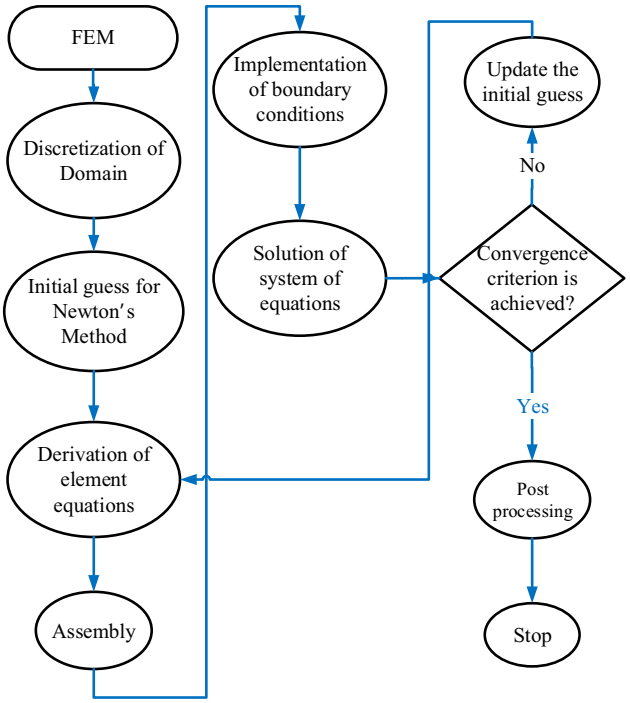

Fig. 1 Flow chart of the finite element method

$$\gamma'' - Le\left[h\gamma - f\gamma' + A\left(\frac{\eta}{2}\gamma' + 2\gamma\right)\right] + \frac{Nt}{Nb}\theta'' = 0, \tag{22}$$

with following boundary condition

$$f(0) = f_w, h(0) = 1 + S_f h'(0), \theta(0) = 1 + S_t\theta'(0),$$
$$S(0) = 1 + S_p S'(0), \gamma(0) = 1 + S_g\gamma'(0), \tag{23}$$

$$h(\infty) \to 0, \theta(\infty) \to 0, S(\infty) \to 0, \gamma(\infty) \to 0, \tag{24}$$

For calculation purposes, the parameter η at ∞ is chosen large enough. The numerical solution therefore has no discernible variation for *eta* greater than η_{max}. Depending on the limit condition, η_{max} is set to $\eta_{max} = 10$.

3.1 Variational formulations

The variational form associated with Eqs. (13)–(18) over a quadratic element $\Omega_e = (\eta_e, \eta_{e+1})$ is given by

$$\int_{\eta_e}^{\eta_{e+1}} s_1\{f' - h\}d\eta = 0, \tag{25}$$

$$\int_{\eta_e}^{\eta_{e+1}} s_2\{h'' + \beta(2hh'' - h'^2 - fh''') + (1+\lambda)(fh' - h^2 - A\left[\frac{\eta}{2}h' + h\right] \tag{26}$$

$$- Mh + \lambda_1\theta + \lambda_2 S + \lambda_3\gamma)\}d\eta = 0, \tag{27}$$

$$\int_{\eta_e}^{\eta_{e+1}} s_3\{(1+R)\frac{1}{Pr}\theta'' - h\theta + f\theta' - A\left(\frac{\eta}{2}\theta' + 2\theta\right) + Nb\gamma'\theta' + Nt\theta'^2 - Mh\}d\eta = 0, \tag{28}$$

$$\int_{\eta_e}^{\eta_{e+1}} s_4\{\frac{1}{Sc}S'' - hS + fS' - A\left(\frac{\eta}{2}S + 2S\right) + S_r\theta''\}d\eta = 0, \tag{29}$$

$$\int_{\eta_e}^{\eta_{e+1}} s_5\{\gamma'' - Le\left[h\gamma - f\gamma' + A\left(\frac{\eta}{2}\gamma' + 2\gamma\right)\right] + \frac{Nt}{Nb}\theta''\}d\eta = 0, \tag{30}$$

where s_1, s_2, s_3, s_4 and s_5 functions are of arbitrary form or test functions.

3.2 Finite element formulations

The equations of the finite element model is obtained by replacing the finite element approach of the following form in Eqs. (19)–(23).

$$f = \sum_{j=1}^{3} f_j\psi_j,\ h = \sum_{j=1}^{3} h_j\psi_j,\ \theta = \sum_{j=1}^{3} \theta_j\,\psi_j,$$
$$S = \sum_{j=1}^{3} S_j\psi_j,\ \gamma = \sum_{j=1}^{3} \gamma_j\psi_j, \tag{31}$$

with $s_1 = s_2 = s_3 = s_4 = s_5 = \psi_i (i = 1, 2)$, where the shape function ψ_i for a line element $\Omega_e = (\eta_e, \eta_e + 1)$ are given by

$$\psi_1 = \frac{(\eta_{e+1} - \eta)(\eta_{e+1} + \eta_e - 2\eta)}{(\eta_{e+1} - \eta_e)^2},\ \psi_2 = \frac{4(\eta - \eta_e)(\eta_{e+1} - \eta)}{(\eta_{e+1} - \eta_e)^2},$$
$$\psi_3 = -\frac{(\eta - \eta_e)(\eta_{e+1} + \eta_e - 2\eta)}{(\eta_{e+1} - \eta_e)^2}, \tag{32}$$

The model equations of the finite element method are therefore given by

$$\begin{bmatrix} F^{11} & F^{12} & F^{13} & F^{14} & F^{15} \\ F^{21} & F^{22} & F^{23} & F^{24} & F^{25} \\ F^{31} & F^{32} & F^{33} & F^{34} & F^{35} \\ F^{41} & F^{42} & F^{43} & F^{44} & F^{45} \\ F^{51} & F^{52} & F^{53} & F^{54} & F^{55} \end{bmatrix} \begin{bmatrix} f \\ h \\ \theta \\ S \\ \gamma \end{bmatrix} = \begin{bmatrix} b_1 \\ b_2 \\ b_3 \\ b^4 \\ b^5 \end{bmatrix} \tag{33}$$

where F_{mn} and b_m (m, n = 1, 2, 3, 4, 5) are defined as

$$F_{ij}^{11} = \int_{\eta_e}^{\eta_{e+1}} \psi_i \frac{d\psi_j}{d\eta}d\eta, F_{ij}^{12} = -\int_{\eta_e}^{\eta_{e+1}} \psi_i\psi_j d\eta,\ F_{ij}^{13} = F_{ij}^{14} = 0, F_{ij}^{15} = F_{ij}^{21} = 0,$$

$$F_{ij}^{22} = -\int_{\eta_e}^{\eta_{e+1}} \frac{d\psi_i}{d\eta}\frac{d\psi_j}{d\eta}d\eta - \beta\int_{\eta_e}^{\eta_{e+1}} \bar{h}\frac{d\psi_i}{d\eta}\frac{d\psi_j}{d\eta}d\eta - 2\beta\int_{\eta_e}^{\eta_{e+1}} \bar{h}'\psi_i\frac{d\psi_j}{d\eta}d\eta + \beta\int_{\eta_e}^{\eta_{e+1}} \frac{d\psi_i}{d\eta}\bar{f}\frac{d^2\psi_j}{d\eta^2}d\eta$$
$$+ \beta\int_{\eta_e}^{\eta_{e+1}} \psi_i\bar{f}'\frac{d^2\psi_j}{d\eta^2}d\eta + (1+\lambda)\int_{\eta_e}^{\eta_{e+1}} \psi_i\bar{f}\frac{d^2\psi_j}{d\eta^2}d\eta - (1+\lambda)\int_{\eta_e}^{\eta_{e+1}} \bar{h}\psi_i\psi_j d\eta - A\frac{\eta}{2}(1+\lambda)\int_{\eta_e}^{\eta_{e+1}} \psi_i\frac{d\psi_j}{d\eta}d\eta$$
$$- 2A(1+\lambda)\int_{\eta_e}^{\eta_{e+1}} \psi_i\psi_j d\eta - M(1+\lambda)\int_{\eta_e}^{\eta_{e+1}} \psi_i\psi_j d\eta$$

$$F_{ij}^{23} = (1+\lambda)\lambda_1\int_{\eta_e}^{\eta_{e+1}} \psi_i\psi_j d\eta, F_{ij}^{24} = (1+\lambda)\lambda_2\int_{\eta_e}^{\eta_{e+1}} \psi_i\psi_j d\eta, F_{ij}^{25} = (1+\lambda)\lambda_3\int_{\eta_e}^{\eta_{e+1}} \psi_i\psi_j d\eta,$$

$$F_{ij}^{31} = 0,\quad F_{ij}^{32} = -M\int_{\eta_e}^{\eta_{e+1}} \psi_i\psi_j d\eta, F_{ij}^{33} = -(1+R)\frac{1}{Pr}\int_{\eta_e}^{\eta_{e+1}} \frac{d\psi_i}{d\eta}\frac{d\psi_j}{d\eta}d\eta - \int_{\eta_e}^{\eta_{e+1}} \bar{h}\psi_i\psi_j d\eta + \int_{\eta_e}^{\eta_{e+1}} \bar{f}\psi_i\frac{d\psi_j}{d\eta}d\eta$$
$$- A\frac{\eta}{2}\int_{\eta_e}^{\eta_{e+1}} \psi_i\frac{d\psi_j}{d\eta}d\eta - 2A\int_{\eta_e}^{\eta_{e+1}} \psi_i\psi_j d\eta + Nb\int_{\eta_e}^{\eta_{e+1}} \bar{\gamma}'\psi_i\frac{d\psi_j}{d\eta}d\eta + Nt\int_{\eta_e}^{\eta_{e+1}} \bar{\theta}'\psi_i\frac{d\psi_j}{d\eta}d\eta,\quad F_{ij}^{34} = 0, F_{ij}^{35} = 0,$$

$$F_{ij}^{41} = F_{ij}^{42} = 0, F_{ij}^{43} = -Sr\int_{\eta_e}^{\eta_{e+1}} \frac{d\psi_i}{d\eta}\frac{d\psi_j}{d\eta}d\eta, F_{ij}^{44} = -\frac{1}{Sc}\int_{\eta_e}^{\eta_{e+1}} \frac{d\psi_i}{d\eta}\frac{d\psi_j}{d\eta}d\eta + \int_{\eta_e}^{\eta_{e+1}} \bar{f}\psi_i\frac{d\psi_j}{d\eta}d\eta - \int_{\eta_e}^{\eta_{e+1}} \bar{h}\psi_i\psi_j d\eta d\eta$$
$$- A\frac{\eta}{2}\int_{\eta_e}^{\eta_{e+1}} \psi_i\frac{d\psi_j}{d\eta}d\eta - 2A\int_{\eta_e}^{\eta_{e+1}} \psi_i\psi_j d\eta,$$

$$F_{ij}^{45} = F_{ij}^{51} = F_{ij}^{52} = F_{ij}^{54} = 0, F_{ij}^{53} = -\frac{Nt}{Nb}\int_{\eta_e}^{\eta_{e+1}} \frac{d\psi_i}{d\eta}\frac{d\psi_j}{d\eta}d\eta\quad F_{ij}^{55} = -\int_{\eta_e}^{\eta_{e+1}} \frac{d\psi_i}{d\eta}\frac{d\psi_j}{d\eta}d\eta$$
$$+ Le\int_{\eta_e}^{\eta_{e+1}} \bar{f}\psi_i\frac{d\psi_j}{d\eta}d\eta - Le\int_{\eta_e}^{\eta_{e+1}} \bar{h}\psi_i\psi_j d\eta d\eta - LeA\frac{\eta}{2}\int_{\eta_e}^{\eta_{e+1}} \psi_i\frac{d\psi_j}{d\eta}d\eta - 2LeA\int_{\eta_e}^{\eta_{e+1}} \psi_i\psi_j d\eta, \tag{34}$$

and

$$b_i^1 = 0,\ b_i^2 = -\left(\psi \frac{dh}{d\eta}\right)_{\eta_e}^{\eta_e+1},$$
$$b_i^3 = -(1+R)\frac{1}{Pr}\left(\psi \frac{d\theta}{d\eta}\right)_{\eta_e}^{\eta_e+1},$$
$$b_i^4 = -\frac{1}{Sc}\left(\psi \frac{dS}{d\eta}\right)_{\eta_e}^{\eta_e+1} - Sr\left(\psi \frac{dS}{d\eta}\right)_{\eta_e}^{\eta_e+1}, \quad (35)$$
$$b_i^5 = -\left(\psi \frac{d\phi}{d\eta}\right)_{\eta_e}^{\eta_e+1} - \frac{Nt}{Nb}\left(\psi \frac{d\theta}{d\eta}\right)_{\eta_e}^{\eta_e+1},$$

where $\bar{f} = \sum_{j=1}^{3} \bar{f}_j \psi_j$, $\bar{h} = \sum_{j=1}^{3} \bar{h}_j \psi_j$, $\bar{\theta}' = \sum_{j=1}^{3} \bar{\theta}'_j \psi_j$ and $\bar{\phi}' = \sum_{j=1}^{3} \bar{\phi}'_j \psi_j$ are supposed to be known. Hence after assembling all the element equations, we get the order of 722×722 matrix. The resulting system is nonlinear, therefore an iterative scheme is utilized in the solution. After the boundary conditions are applied, the remaining system equations are solved by gaussian elimination method and will repeat this process until the desired accuracy of 0.00005 obtained.

4 Results

The velocity distribution decreases with the increment of magnetic parameter M with suction, injunction and no suction in the presence of hydrodynamic slip S_f and absence of hydrodynamic slip S_f are depicted in Fig. 2. With the enhancing of viscoelastic parameter β and presence/absence of unsteadiness parameter A effects on increasing the velocity profile with both cases of hydrodynamic and no hydrodynamic slip are discussed in Fig. 3.

In the absence and presence of the unsteady parameter A, the radiation R and the hydrodynamic slip condition S_f, the velocity profile is enhanced as the buoyancy parameters λ_1, λ_2 and λ_3 increases, the results are described graphically in Figs. 4, 5 and 6. The influence of thermal radiation

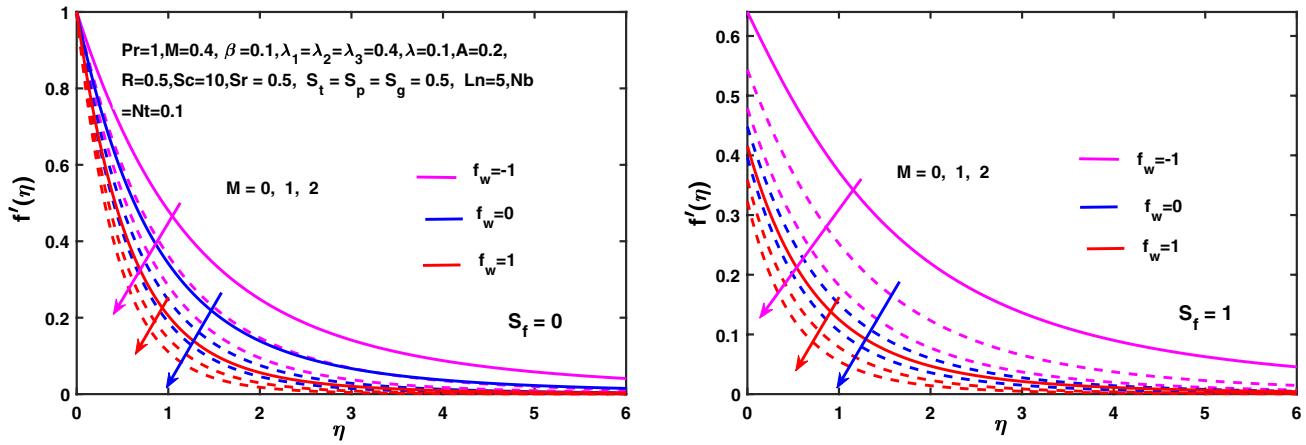

Fig. 2 Effect of M and f_w on velocity distribution with slip and no slip condition S_f

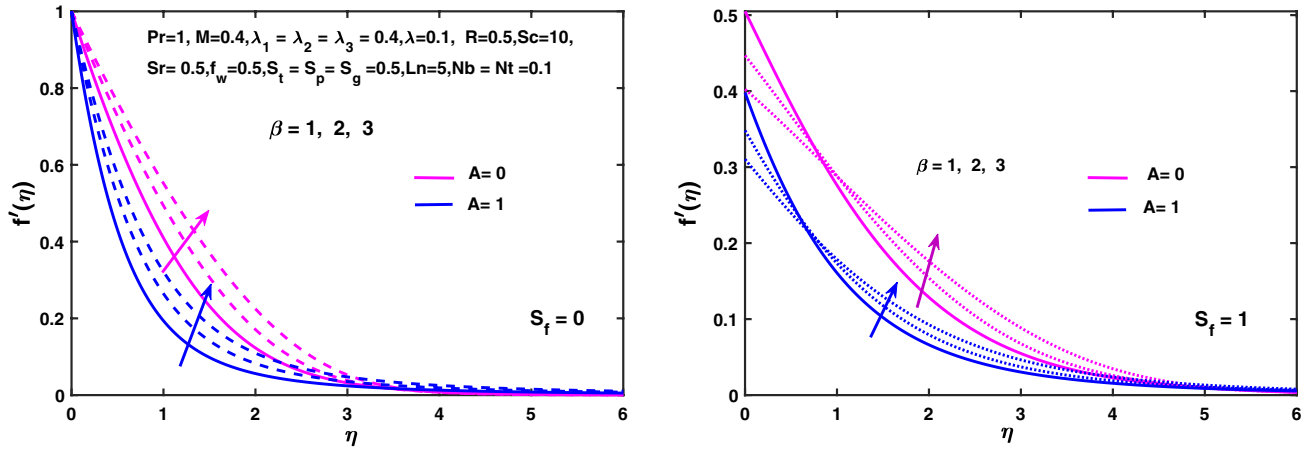

Fig. 3 Effect of β and A on velocity distribution with slip and no slip condition S_f

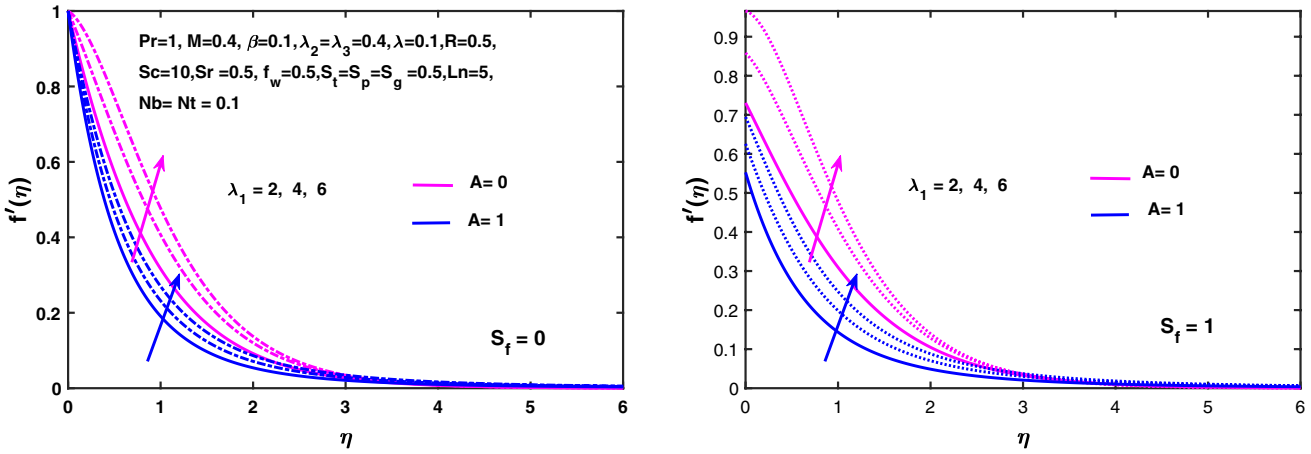

Fig. 4 Effect of λ_1 and A on velocity distribution with slip and no slip condition S_f

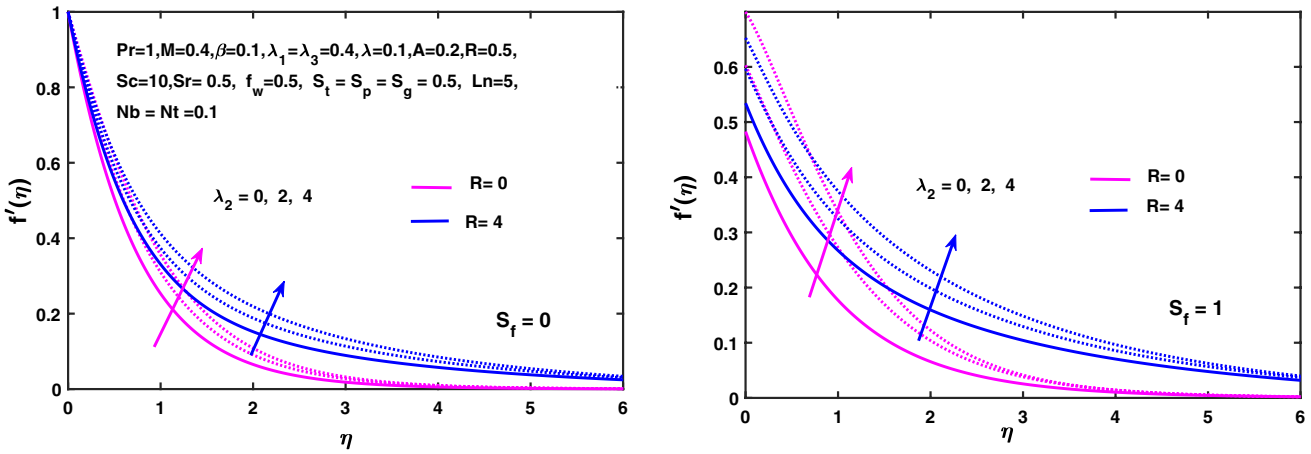

Fig. 5 Effect of λ_2 and R on velocity distribution with slip and no slip condition S_f

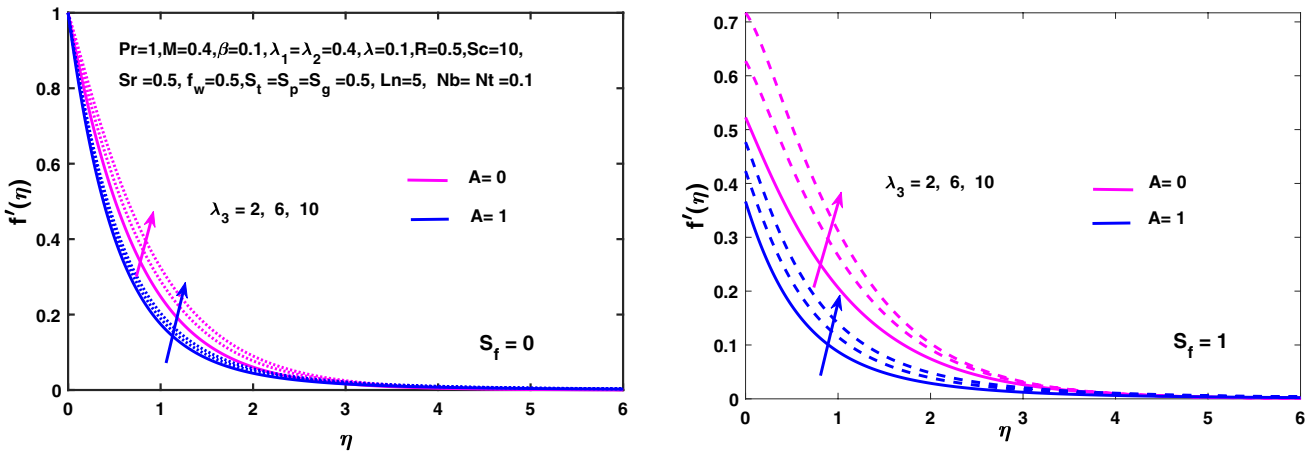

Fig. 6 Effect of λ_3 and A on velocity distribution with slip and no slip condition S_f

R and magnetic parameter M with thermal slip and no thermal slip condition are presented in the Fig. 7, applying the magnetic field heats up the fluid and thus reduces the heat and mass transfer rates from the wall causing increases in fluid temperature. We noticed from Fig. 7 that the temperature profile increases as the radiation

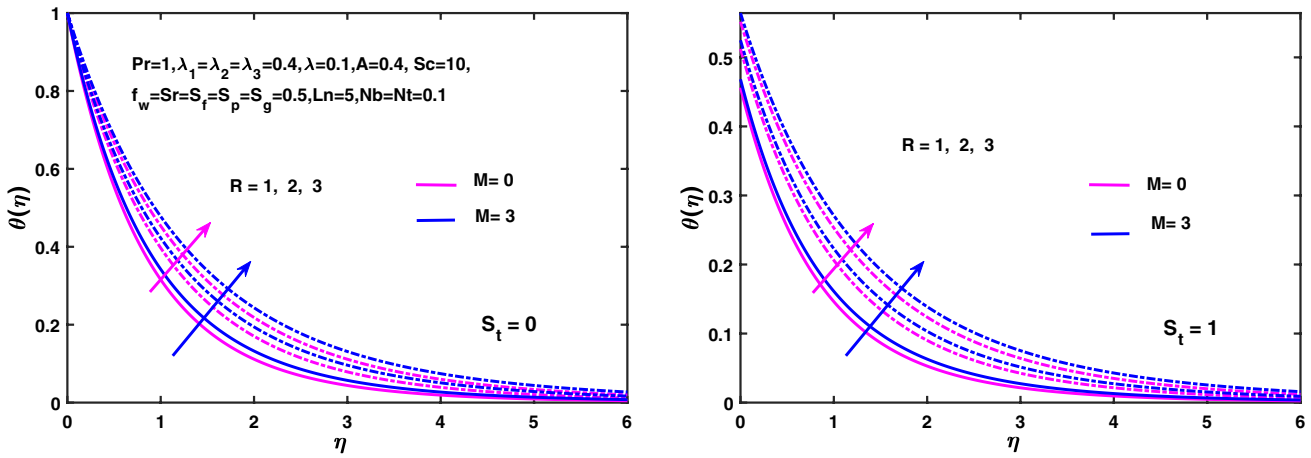

Fig. 7 Effect of *R* and *M* on temperature profile with slip and no slip condition S_t

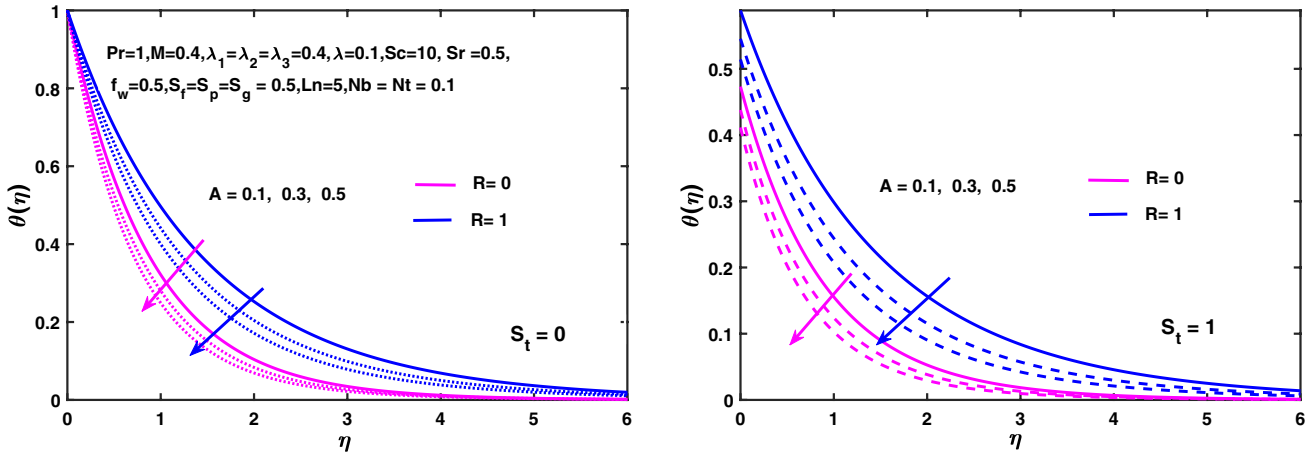

Fig. 8 Effect of *A* and *R* on temperature profile with slip and no slip condition S_t

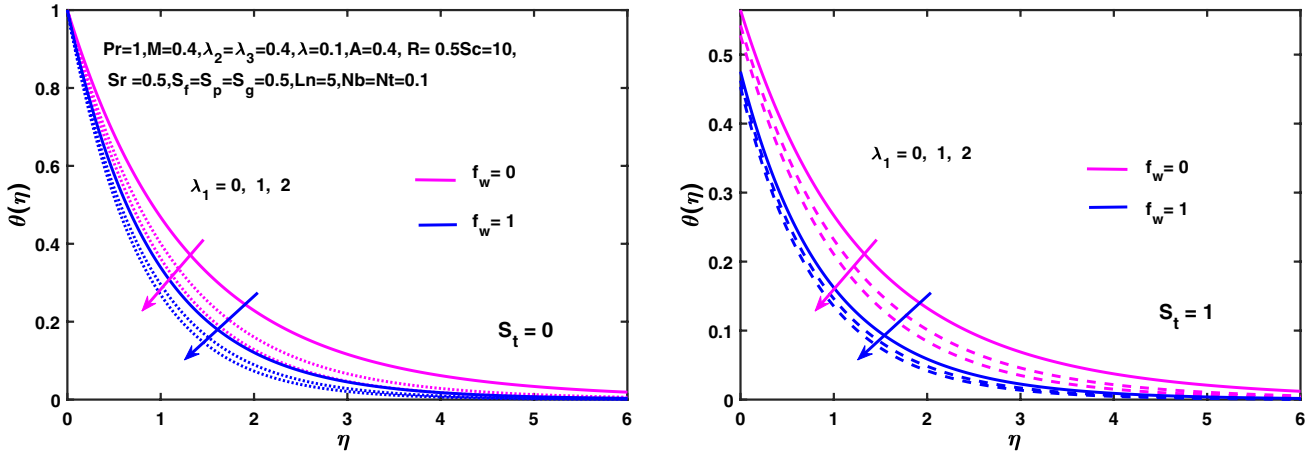

Fig. 9 Effect of λ_1 and f_w on temperature profile with slip and no slip condition S_t

parameter *R* value increases. Figures 8 and 9 depict that the temperature decreases as the effect of unsteadiness *A* increases with the presence and absence of the radiation parameter *R* and thermal slip condition S_t. The temperature profile increases as the thermophoresis parameter increase with presence and absence of suction f_w and

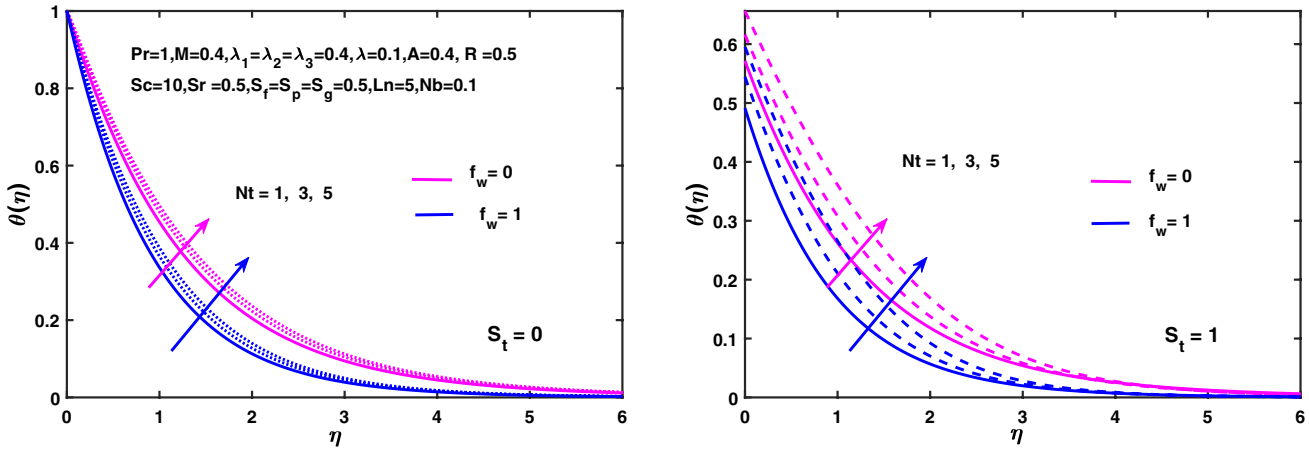

Fig. 10 Effect of *Nt* and f_w on temperature profile with slip and no slip condition S_t

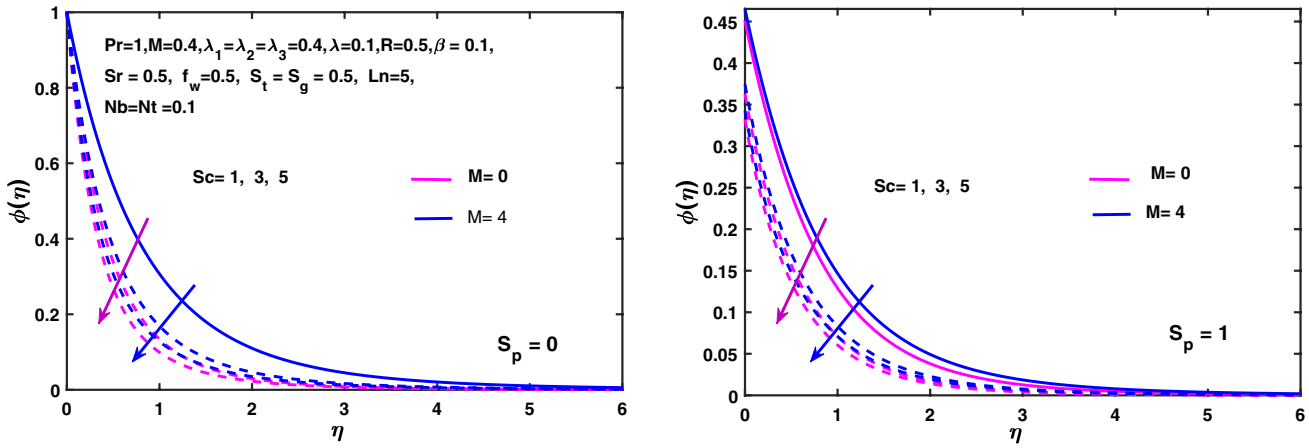

Fig. 11 Effect of *Sc* and *M* on concentration profile with slip and no slip condition S_p

thermal slip parameter S_t, as described in Fig. 10. The effect of the Schmidt number *Sc* and the magnetic parameter *M* on the concentration distribution is shown in Fig. 11. We observed that as the Schmidt number increases, the concentration distribution retard with the presence and absence of solute slip S_p. Figure 12 presents the characteristics of the *Sr* Soret number and the *A* instability with the presence and absence of an absolute S_p slip on the concentration profile. It is clear from the figure that the intensification of the Soret number has reinforced the concentration profile and the associated concentration boundary layer.

Figure 13 describes the characteristics of the Lewis number and the instability of *A* on the nano-liquid slip profile without nano-liquid slip conditions. It is from the figure that the intensification the Lewis number reduces the volume fraction profile of nanofluid. Moreover, when we increase the value of the Lewis number, the concentration field is reduced because it is inversely proportional to the Brownie coefficient. The Brown diffusion coefficient is low for higher Lewis numbers and the Brown diffusion coefficient results in a decrease in the concentration field. Figure 14 is ready to take action, the *Nb* Brownian motion parameter and the f_w suction parameter with the presence and absence of nano-fluid slip on the friction profile of the nano-fluid volume. The figure clearly shows that the volume friction profile of the nano-fluid and the associated boundary layer thickness of the nanoparticle concentration accumulate for a higher parameter for Brownian motion. Figure 15 describe the influences of *A*, *M*, S_f, *R*, *Nt* and S_t, on velocity and temperature gradients. Effects of *M*, *A* and S_f on skin friction (C_f) are portrayed in Fig. 15a. As previously seen, the fluid velocity decreases by increasing the magnetic parameter due to the Lorentz force caused by the magnetic field; as a result, the rubbing of the skin shows a behavior for the higher magnetic parameter, as shown in this figure. Skin friction diminish for *M* with increasing the unsteady parameter *A*. Figure 15b shows the impacts of *Nt*, S_t and *R* on temperature gradient (*Nu*).

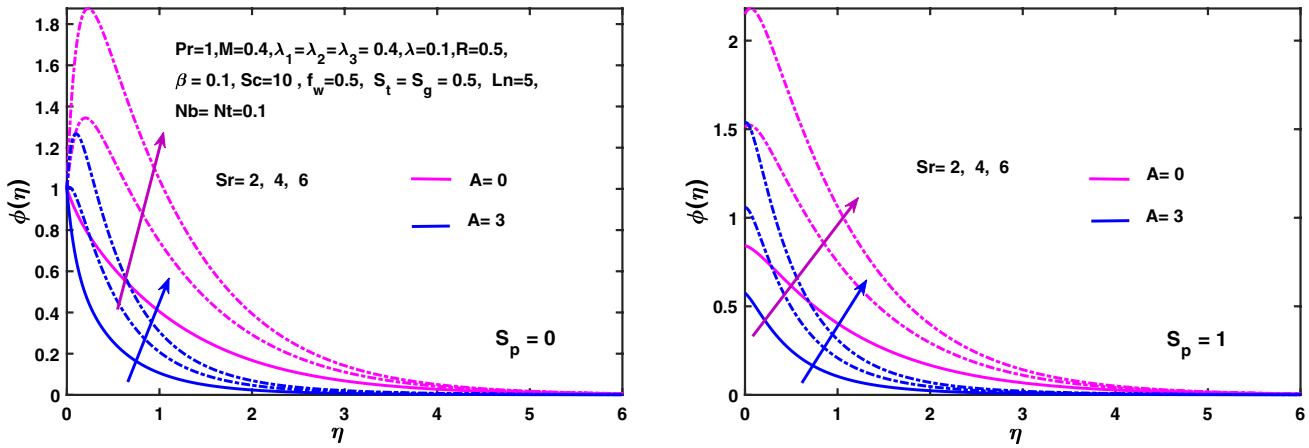

Fig. 12 Effect of *Sr* and *A* on concentration profile with slip and no slip condition S_p

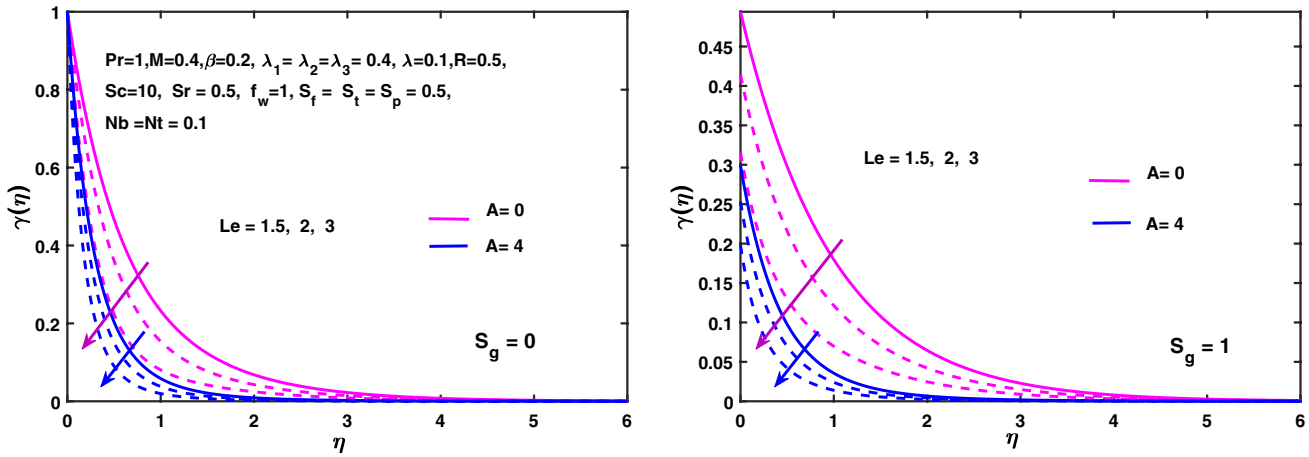

Fig. 13 Effect of *Le* and *A* on nanofluid volume fraction profile with slip and no slip condition S_g

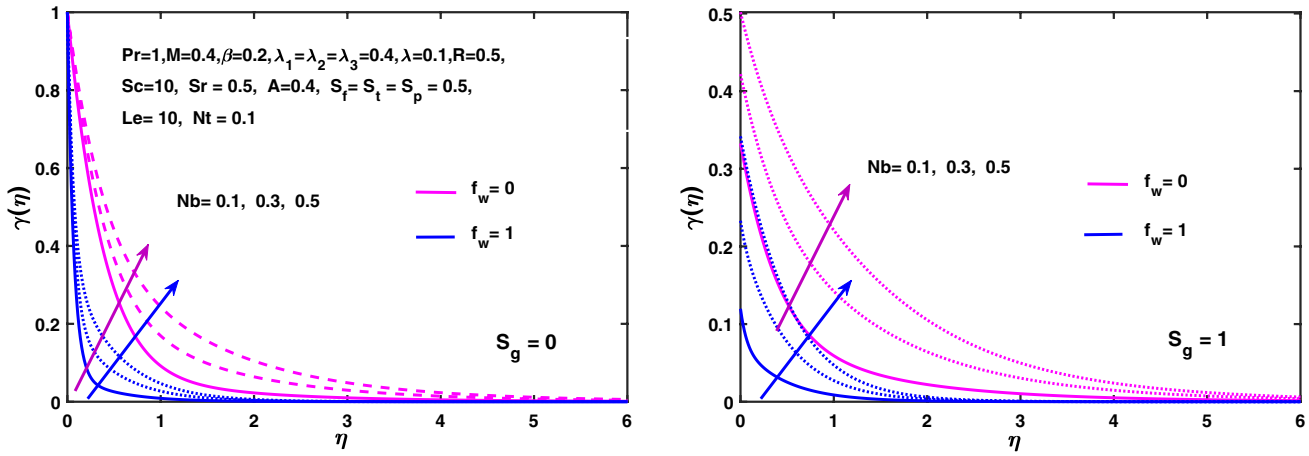

Fig. 14 Effect of *Nb* and f_w on nano-fluid volume fraction profile with slip and no slip condition S_g

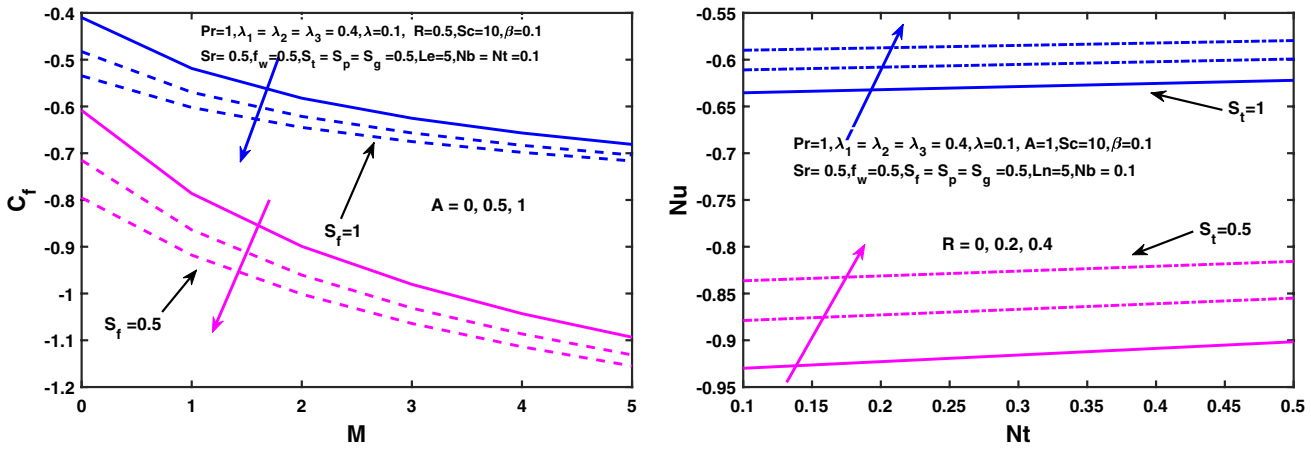

Fig. 15 Effect of M,S_f and A on skin friction coefficient C_f, and effect of Nt, R and S_t on Nusselt number

These plots show that the the heat transfer rate decreases with the growth of the thermophoresis parameter. This is due to the fact that a larger one the thermophoretic force drives nanoparticles with high thermal conductivity from the hottest region to the ambient temperature liquid. Nano-scale thermophoresis therefore has a considerable influence on the behavior of heat transfer at plate level. Further, increasing the values of R the temperature gradient increases.

Table 2 Comparison of $-f''(0)$ for various values of A when $M = f_w = S_f = \lambda_1 = \lambda_2 = 0$

σ	Chamkha et al. [44]	Fazle [42]	FEM (present)
0.8	1.261512	1.261042	1.261042
1.2	1.378052	1.377724	1.377724

5 Discussion

A theoretical study was conducted to investigate the nanofluidic flux induced by a stretching surface [46]. It was probably the first attempt to reflect the flow of nanofluids on a stretch sheet using the Buongiorno model. Later Makinde and Aziz [47] investigated the effects of convective heat transfer in the nanofluid flow on the boundary layer on a flat plate. Recently, Hashim and Khan [48] studied the heat and mass transfer characteristics for the flow of Carreau nanofluids past a stretching surface. Multiple slip effects on MHD unsteady flow heat and mass transfer impinging on permeable stretching sheet with radiation was discussed [42] and found that the existence of the hydrodynamic slip increases the velocity boundary layer. Here, we focused on describing the effects of different flow variables on velocity distribution ($f'(\eta)$), temperature profile ($\theta(\eta)$), concentration ($S(\eta)$), nano-fluid volume fraction profile ($\gamma(\eta)$), skin friction (C_f), Nusselt number (Nu), Sherwood number Sh_x and nano-particle Sherwood number ($Sh_{x,n}$). The nonlinear systems (18)–(22) subject to conditions (23) and (24) are solved numerically by hybrid finite element method. Further the characteristics of magnetic M, Brownian Nb,

Table 1 Comparison of $-f''(0)$ for various values of M when $f_w = A = S_f = 0$ and Pr when $M = f_w = S_f = S_t = A = \lambda_1 = \lambda_2 = R = 0$

M	Mabood and Das [41]	Fazle [42]	FEM (present)	Pr	Ali [43]	FEM (present)
0	− 1.000008	− 1.0000024	− 1.0000062	–	–	–
1	1.4142145	1.41421316	1.41421563	–	–	–
5	2.4494867	2.44948944	2.44943463	0.72	0.8058	0.8088
10	3.3166237	3.31662459	3.31664163	1	0.9691	1.0000
50	7.1414294	7.14142833	7.14141539	3	1.9144	1.9237
100	10.049855	10.0498776	10.0498451	10	3.7006	3.7207
500	22.383049	22.3830203	22.3830323	–	–	–
1000	31.638574	31.6385890	31.6385753	–	–	–

Table 3 Comparison of $-\theta'(0)$ for various values of Pr ($M = f_w = S_\theta = \sigma = \lambda_1 = \lambda_2 = \lambda_3 = R = S_f = 0$;)

Pr	Aii [43]	Fazle and Stanford [42]	Ishak et al. [45]	Ishak et al. [45]	FEM	Error in %
				Exact solution (a)	Present results (b)	$\left\|\left(\frac{b-a}{a}\right)\right\| \times 100$
0.72	0.8058	0.8088	–	0.8086313498	0.8086339299	0.0003
1.00	0.9691	1.0000	1.0000	1.000000000	1.0000080213	0.0008
3.00	1.9144	1.9237	1.9237	1.923682594	1.9236777221	0.0003
10.0	3.7006	3.7207	3.7207	3.720673901	3.7206681683	0.0002
100	–	–	12.2941	12.294083260	12.294051659	0.0003

thermophoresis Nt, Schmidt Sc, Lewis number Le, thermal radiation R,Soret number Sr, unsteady parameter A, Buoyancy parameters λ_1, λ_2, λ_3, Deborah number or viscoelastic parameter β, hydrodynamic slip S_f, thermal slip S_t, solutal slip S_p and the nano-particle slip condition S_g are presented in this section. The numerical method is validated with the result obtained by Mabood and Das [41], Fazle mabood and Stanford Shateyi [42], Mudassar et al.[49], Gireesha et al. [50], Ishak et al.[45], Ali [43] and Chamkha et al.[44] in terms of skin friction coefficient and an excellent agreement is obtained, the comparison is illustrated in Tables 1, 2 and 3.

6 Conclusions

Here we explored a mathematical model to simulate an unsteady two-dimensional magnetohydrodynamic viscoelastic nano-fluid flow of an incompressible electrically conducting fluid over a permeable stretching sheet in the presence of multiple slips, Soret, and thermal radiation effect. The major results are listed below:

- The boundary layers increases in the presence of multiple slips.
- The velocity distribution boosts via viscoelastic parameter (β) and buoyancy parameters (λ_1, λ_2, λ_3), and decrease with increase of magnetic parameter (M).
- Temperature decays through unsteady parameter (A) and buoyancy parameter (λ_1), while it enhanced with radiation (R) and thermophoresis parameter (Nt).
- Concentration profile enhance via increasing the Soret number (Sr) and diminish with Schmidt number (Sc).
- For larger estimation of Brownian motion parameter (Nb) the nano-fluid volume fraction profile enhance however it is reduced for Lewis number (Le).
- Skin friction coefficient shows decreasing behaviour against unsteadiness (A)and magnetic parameter (M).
- Nusselt number shows increasing behaviour against radiation parameter (R) and thermophoresis parameter (Nt).
- Sherwood number (Sh_x) is increasing function of Schmidt number (Sc) and magnetic parameter (M).
- Nano-particle Sherwood number ($Sh_{x,n}$) is enhanced as a function of thermophoresis parameter (Nt) with increasing value of unsteadiness parameter (A).

Funding This research was funded by National Natural Science Foundation of China No. 11971386.

Compliance with ethical standards

Conflict of interest The authors declare no conflict of interest.

References

1. Khan SU, Ali N, Sajid M, Hayat T (2018) Heat transfer characteristics in oscillatory hydromagnetic channel flow of Maxwell fluid using Cattaneo–Christov model. Proc Natl Acad Sci India Sect A Phys Sci 89:1–9
2. Basha HT, Makinde OD, Arora A, Singh A, Sivaraj R (2018) Unsteady flow of chemically reacting nanofluid over a cone and plate with heat source/sink. In: Defect and diffusion forum, vol 387. Trans Tech Publications, pp 615–624
3. Dash G, Ojha KL (2018) Viscoelastic hydromagnetic flow between two porous parallel plates in the presence of sinusoidal pressure gradient. Alex Eng J 57(4):3463–3471
4. Sheikholeslami M, Ganji D (2017) Transportation of mhd nanofluid free convection in a porous semi annulus using numerical approach. Chem Phys Lett 669:202–210
5. Akbar NS, Tripathi D, Khan ZH, Bég OA (2016) A numerical study of magnetohydrodynamic transport of nanofluids over a vertical stretching sheet with exponential temperature-dependent viscosity and buoyancy effects. Chem Phys Lett 661:20–30
6. Ahmed SE, Aly AM, Raizah Z (2019) Heat transfer enhancement from an inclined plate through a heat generating and variable porosity porous medium using nanofluids due to solar radiation. SN Appl Sci 1(7):661
7. Hassan AR, Fenuga OJ (2019) The effects of thermal radiation on the flow of a reactive hydromagnetic heat generating couple stress fluid through a porous channel. SN Appl Sci 1(10):1278
8. EL-Dabe NT, Attia HA, Essawy MA, Abd-elmaksoud IH, Ramadan AA, Abdel-Hamid AH (2019) Non-linear heat and mass transfer

in a thermal radiated mhd flow of a power-law nanofluid over a rotating disk. SN Appl Sci 1(6):551
9. Shit G, Haldar R, Ghosh S (2016) Convective heat transfer and MHD viscoelastic nanofluid flow induced by a stretching sheet. Int J Appl Comput Math 2(4):593–608
10. Sheikholeslami M, Shamlooei M (2017) Fe_3O_4–H_2O nanofluid natural convection in presence of thermal radiation. Int J Hydrog Energy 42(9):5708–5718
11. Sheikholeslami M, Zeeshan A (2017) Analysis of flow and heat transfer in water based nanofluid due to magnetic field in a porous enclosure with constant heat flux using cvfem. Comput Methods Appl Mech Eng 320:68–81
12. Sheikholeslami M, Vajravelu K (2017) Nanofluid flow and heat transfer in a cavity with variable magnetic field. Appl Math Comput 298:272–282
13. Hussanan A, Salleh MZ, Khan I, Shafie S (2018) Analytical solution for suction and injection flow of a viscoplastic casson fluid past a stretching surface in the presence of viscous dissipation. Neural Comput Appl 29(12):1507–1515
14. Majeed A, Zeeshan A, Alamri SZ, Ellahi R (2018) Heat transfer analysis in ferromagnetic viscoelastic fluid flow over a stretching sheet with suction. Neural Comput Appl 30(6):1947–1955
15. Ellahi R (2013) The effects of mhd and temperature dependent viscosity on the flow of non-newtonian nanofluid in a pipe: analytical solutions. Appl Math Model 37(3):1451–1467
16. Choi SU, Eastman JA (1995) Enhancing thermal conductivity of fluids with nanoparticles. Technical report, Argonne National Lab, IL (United States)
17. Buongiorno J (2006) Convective transport in nanofluids. J Heat Transf 128(3):240–250
18. Sheikholeslami M, Arabkoohsar A, Jafaryar M (2019) Impact of a helical-twisting device on the thermal–hydraulic performance of a nanofluid flow through a tube. J Therm Anal Calorim. https://doi.org/10.1007/s10973-019-08683-x
19. Sheikholeslami M, Jafaryar M, Ali JA, Hamad SM, Divsalar A, Shafee A, Nguyen-Thoi T, Li Z (2019) Simulation of turbulent flow of nanofluid due to existence of new effective turbulator involving entropy generation. J Mol Liq 291:111283
20. Sheikholeslami M (2018) Numerical modeling of nano enhanced PCM solidification in an enclosure with metallic fin. J Mol Liq 259:424–438
21. Sheikholeslami M (2018) Influence of magnetic field on Al_2O_3 –H_2O nanofluid forced convection heat transfer in a porous lid driven cavity with hot sphere obstacle by means of lbm. J Mol Liq 263:472–488
22. Sheikholeslami M (2018) Finite element method for pcm solidification in existence of cuo nanoparticles. J Mol Liq 265:347–355
23. Sheikholeslami M, Jafaryar M, Shafee A, Li Z, Haq R-U (2019) Heat transfer of nanoparticles employing innovative turbulator considering entropy generation. Int J Heat Mass Transf 136:1233–1240
24. Sulochana C, Samrat S, Sandeep N (2018) Magnetohydrodynamic radiative liquid thin film flow of kerosene based nanofluid with the aligned magnetic field. Alex Eng J 57(4):3009–3017
25. Daniel YS, Aziz ZA, Ismail Z, Salah F (2018) Effects of slip and convective conditions on mhd flow of nanofluid over a porous nonlinear stretching/shrinking sheet. Aust J Mech Eng 16(3):213–229
26. Shiriny A, Bayareh M, Nadooshan AA (2019) Nanofluid flow in a microchannel with inclined cross-flow injection. SN Appl Sci 1(9):1015
27. Hakeem A, Nayak M, Makinde O (2019) Effect of exponentially variable viscosity and permeability on blasius flow of carreau nano fluid over an electromagnetic plate through a porous medium. J Appl Comput Mech 5(2):390–401
28. Waqas M, Khan MI, Hayat T, Farooq S, Alsaedi A (2019) Interaction of thermal radiation in hydromagnetic viscoelastic nanomaterial subject to gyrotactic microorganisms. Appl Nanosci 9:1–12
29. Maleki H, Alsarraf J, Moghanizadeh A, Hajabdollahi H, Safaei MR (2019) Heat transfer and nanofluid flow over a porous plate with radiation and slip boundary conditions. J Cent South Univ 26(5):1099–1115
30. Alamri SZ, Ellahi R, Shehzad N, Zeeshan A (2019) Convective radiative plane poiseuille flow of nanofluid through porous medium with slip: an application of stefan blowing. J Mol Liq 273:292–304
31. Besthapu P, Haq RU, Bandari S, Al-Mdallal QM (2019) Thermal radiation and slip effects on mhd stagnation point flow of non-newtonian nanofluid over a convective stretching surface. Neural Comput Appl 31(1):207–217
32. Khan SA, Nie Y, Ali B (2019) Multiple slip effects on magnetohydrodynamic axisymmetric buoyant nanofluid flow above a stretching sheet with radiation and chemical reaction. Symmetry 11(9):1171
33. Ali B, Nie Y, Khan SA, Sadiq MT, Tariq M (2019) Finite element simulation of multiple slip effects on mhd unsteady maxwell nanofluid flow over a permeable stretching sheet with radiation and thermo-diffusion in the presence of chemical reaction. Processes 7(9):628
34. Uddin M, Rana P, Bég OA, Ismail AM (2016) Finite element simulation of magnetohydrodynamic convective nanofluid slip flow in porous media with nonlinear radiation. Alex Eng J 55(2):1305–1319
35. Bhargava R, Chandra H. Numerical simulation of MHD boundary layer flow and heat transfer over a nonlinear stretching sheet in the porous medium with viscous dissipation using hybrid approach. arXiv preprint arXiv:1711.03579
36. Goyal M, Bhargava R (2013) Numerical solution of MHD viscoelastic nanofluid flow over a stretching sheet with partial slip and heat source/sink. ISRN Nanotechnol 2013:931021
37. Madhu M, Kishan N (2015) Finite element analysis of mhd viscoelastic nanofluid flow over a stretching sheet with radiation. Procedia Eng 127:432–439
38. Bhargava R, Rana P (2011) Finite element solution to mixed convection in mhd flow of micropolar fluid along a moving vertical cylinder with variable conductivity. Int J Appl Math Mech 7:29–51
39. Lin Y-Y, Lo S-P (2003) Finite element modeling for chemical mechanical polishing process under different back pressures. J Mater Process Technol 140(1–3):646–652
40. Dettmer W, Perić D (2006) A computational framework for fluid–rigid body interaction: finite element formulation and applications. Comput Methods Appl Mech Eng 195(13–16):1633–1666
41. Mabood F, Das K (2016) Melting heat transfer on hydromagnetic flow of a nanofluid over a stretching sheet with radiation and second-order slip. Eur Phys J Plus 131(1):3
42. Mabood F, Shateyi S (2019) Multiple slip effects on MHD unsteady flow heat and mass transfer impinging on permeable stretching sheet with radiation. Modelling and Simulation in Engineering
43. Ali ME (1994) Heat transfer characteristics of a continuous stretching surface. Wärme-und Stoffübertragung 29(4):227–234
44. Chamkha A, Aly A, Mansour M (2010) Similarity solution for unsteady heat and mass transfer from a stretching surface embedded in a porous medium with suction/injection and chemical reaction effects. Chem Eng Commun 197(6):846–858
45. Ishak A, Nazar R, Pop I (2009) Boundary layer flow and heat transfer over an unsteady stretching vertical surface. Meccanica 44(4):369–375
46. Khan W, Pop I (2010) Boundary-layer flow of a nanofluid past a stretching sheet. Int J Heat Mass Transf 53(11–12):2477–2483

47. Makinde OD, Aziz A (2011) Boundary layer flow of a nanofluid past a stretching sheet with a convective boundary condition. Int J Therm Sci 50(7):1326–1332
48. Khan M et al (2016) A revised model to analyze the heat and mass transfer mechanisms in the flow of carreau nanofluids. Int J Heat Mass Transf 103:291–297
49. Jalil M, Asghar S, Yasmeen S (2017) An exact solution of MHD boundary layer flow of dusty fluid over a stretching surface. Math Probl Eng 2017:2307469
50. Gireesha B, Ramesh G, Bagewadi C (2012) Heat transfer in mhd flow of a dusty fluid over a stretching sheet with viscous dissipation. J Appl Sci Res 3(4):2392–2401